Evaluating and Quantifying Viability of 3D-Printed Cells with Mathematical Modeling Across Different Bioprinting Methods

A Technical Report submitted to the Department of Biomedical Engineering

Presented to the Faculty of the School of Engineering and Applied Science

University of Virginia • Charlottesville, Virginia

In Partial Fulfillment of the Requirements for the Degree

Bachelor of Science, School of Engineering

Juan Martin Carrasco Carvajal

Spring, 2021

On my honor as a University Student, I have neither given nor received unauthorized aid on this assignment as defined by the Honor Guidelines for Thesis-Related Assignments

George Christ, Department of Biomedical Engineering

Chris Highley, Department of Biomedical Engineering

Evaluating and Quantifying Viability of 3D-Printed Cells with Mathematical Modeling Across Different Bioprinting Methods

Juan Martin Carrasco Carvajal

Abstract

3D-bioprinting has the potential to be a very useful tool in the field of tissue engineering, specifically when it comes to biomanufacturing of tissue engineering medical products. One such example is with tissue engineered muscle repair (TEMR) constructs used to treat volumetric muscle loss (VML). In order to ensure successful integration of 3D-bioprinting in the field of tissue engineering as a biomanufacturing tool, it is necessary to fully understand the printing process and its effects on the printed cells. Currently, it is known that the printing process results in some percentage of cell death largely due to the mechanical stresses induced by the extrusion process. However, full understanding over these stresses and its effects is still needed. In particular, there is a large degree of variability in cell viability between printing parameters and across printing methods. To this end, this project consisted of a quantitative analysis of cell viability using different extrusion-based bioprinting methods and varying nozzle diameters, culminating in mathematical modeling to relate shear stress, nozzle diameter, and cell viability. The project was done in the context of TEMR biofabrication for treating VML. As such, mouse C2C12 cells and human muscle progenitor cells were used along with a hyaluronic acid hydrogel. High cell viability (>98%) for both cell types was achieved using a piston-driven printhead paired with a 0.41mm-diameter nozzle.

Keywords: bioprinting, cell viability, mathematical modeling, tissue engineering, hyaluronic acid

Introduction

Three-dimensional bioprinting is an emerging technology in the field of tissue engineering (TE) and regenerative medicine (RM) that has shown potential as a tool for automated biofabrication of tissue constructs.[1–5] Extrusion-based bioprinting is the most widely used method of printing in the field of TE and RM because of its simplicity and accessibility.[3,6] Many commercially available printers are extrusion-based systems and, in fact, some conventional plastic 3D-printers can be modified to print bioink. This printing method involves the extrusion of cells embedded in a hydrogel bioink through a nozzle in specific pre-determined patterns (Fig. 1D). Here, the term bioink refers to the mixture of a hydrogel biomaterial and encapsulated cells that are used to print tissue constructs.[7] The cell type and biomaterial are dictated by the desired tissue type and properties. Controlling the deposition of cells in this way enables the user to print tissue constructs that mimic the pattern and organization of real tissue structures. There are two popular mechanisms of extrusion with this method: pneumatic extrusion and piston-driven extrusion.[1,3] The difference between these two is illustrated

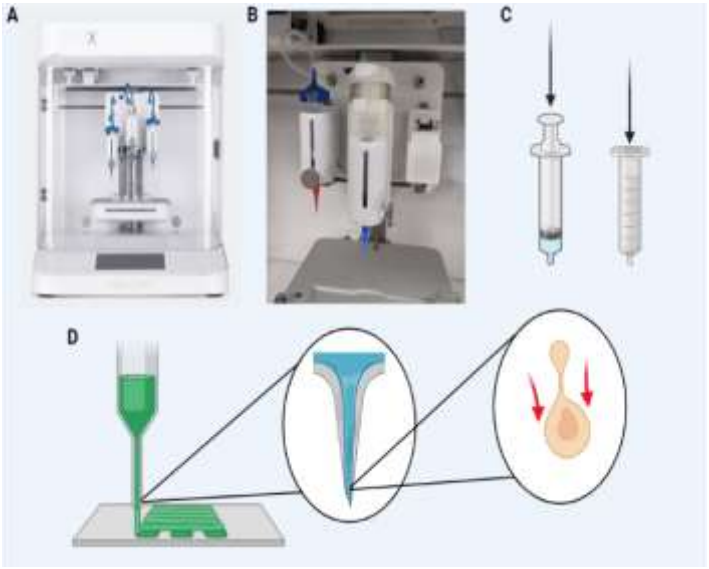

Fig. 1. Extrusion Bioprinting. (A) CellInk BioX printer. (B) Close up of pneumatic (left) and piston (center) printheads. (C) Illustration of piston vs pneumatic extrusion. (D) Illustration of extrusion process and induced shear stress experienced by cells (Created with BioRender.com).

in Fig. 1C, where it can be seen that one is driven by air pressure and the other is driven by a plunger/syringe.

Tissue-engineered muscle repair (TEMR) constructs are a prime example of the potential this technology has to achieve automation, cost and time reduction, and reproducibility in the manufacturing process.[2,5] These constructs, for example, are being explored as novel treatment options for volumetric muscle loss (VML). VML is characterized as a traumatic loss of substantial skeletal muscle volume resulting in permanent functional impairment.[2,8] Current therapies involve multiple reconstructive surgical procedures which often fail to fully restore muscle volume and function, especially in more severe cases often seen in combat veterans.[2] These novel therapies in the field of TE and RM are aimed at aiding the body's regeneration of the lost skeletal muscle. TEMR constructs are typically manufactured by integrating decellularized extracellular matrix (dECM) scaffolds with muscle progenitor cells (MPCs) to promote skeletal muscle regeneration once implanted.[2,5] When constructed manually, the process can take approximately 15-17 days, including a 10-day proliferation period, and requires high cell densities when seeding the MPCs onto the dECM scaffold.[2] However, with bioprinting, confluence on both sides of the dECM sheet is achieved after 24 hours and a lower cell density is required to achieve sufficient cell coverage.[2]

Having established the technical advantages of bioprinting in the context of the TE and RM space, it is important to note that to date there are very few TE/RM products that have been presented to the U.S. Food and Drug Administration (FDA) for approval.[4,5] When designing novel therapeutics such as these for human implantation, it is necessary to understand all aspects of the manufacturing process for the sake of reproducibility and safety. It is known that cells are subjected to many mechanical forces during the extrusion printing process.[3,6,9–12] These compressive, tensile, and shear forces can drive many biological signals and processes such as growth, proliferation, and differentiation. Of particular importance in the field of TE and RM is the effect of bioprinting-induced shear stress on cell viability. The bioprinting process inherently results in some percentage of damaged or dead cells due to the induced mechanical stress upon the cells during extrusion.[3,6,9–12] Implantation of any number of dead cells needs to be accounted for and have a strong rationale in order to ensure successful clinical translation of TEMR constructs.[5] Additionally, the functionality of the tissue construct is highly dependent on the viability of the cells which comprise it.[4,5,11] Therefore, maintaining the highest possible cell viability through the printing process is an essential consideration for biofabricating TEMR constructs for autologous skeletal muscle regeneration following VML. Currently, few studies have sought to quantitatively evaluate the impact of printing methods and printing parameters on cell viability.[1,3,5,12] Though current extrusion-based bioprinting technology can yield viability as high as >90% which surpasses the ISO standard for implanted medical devices, the results may vary with changes in printer models and printing parameters.[1,2,6,13] This highlights the difficulty of balancing printing resolution and cell viability – better resolution induces larger shear stresses and thus damages more cells.[6,11] Reproducibility and greater user control are essential to the clinical success of bioprinted tissue constructs and the integration of bioprinting into the biofabrication process in TE and RM. Thus, there is a need for a more thorough understanding and control over bioprinting's effect on shear stress and and cell viability.

Of particular importance to this investigation is the observable difference in viability between piston and pneumatic printing. In the aforementioned study from the University of Virginia, the authors achieved ~98% cell viability 24h after printing with a Organovo NovoGen 3D bioprinter.[2] Upon reviewing current literature on 3D bioprinting, it is clear that these results are on the high end of the cell viability range which can drop as low as 40% with extrusion-based printing.[14] The Organovo printer is a piston-based printer which differs from most commercially available printers which have pneumatic printheads. With a piston-driven extrusion printhead, the flow rate of the bioink is typically steadier as it is controlled by a syringe that presses down in programmed incremental distances. This consistent flow rate yields consistent deposition of cell-laden bioink. In contrast, pneumatic printing tends to offer less consistent bioink extrusion on account of the delay required to compress the gas. The consistent pressure applied to the bioink could explain why the Organovo system yields such high cell viability. However, this printer is more complex and less user-friendly compared to most commercially available printers. Therefore, the CellInk BioX serves as an ideal investigative platform for this project as it offers both pneumatic and piston printheads while being very user-friendly and commercially available (Fig. 1). This system can provide insights into general extrusion printing and be used to draw comparisons between printing methods and systems.

The present project aims to address the aforementioned knowledge gap with a quantitative analysis of cell viability culminating in mathematical modeling relating nozzle diameter to cell viability and induced shear. The goal of this project is to provide insights that can inform

future experiments with TEMR constructs and introduce a larger degree of control and predictability to future bioprinting for biofabrication. Attempting to model the effect of bioprinting on cell viability is not a new idea, however, existing models are few in number and limited in scope.[3,9,12] The limitations of these models arise from the specific biomedical applications of the studies which dictate cell type, bioink, and printer selection as well as the desired cell viability threshold. As such, existing methods utilize cell types and bioinks that are not necessarily relevant to TEMR and muscular regeneration.[3,9,12] The present project uses C2C12 cells (an immortalized murine skeletal muscle myoblast) , human muscle progenitor cells (hMPCs), and hyaluronic acid (HA) bioink which gives the model relevance and significance in the biofabrication of tissue constructs for muscle regeneration.

Thus, the specific aims of this project were to first conduct a thorough quantitative analysis of viability across the two-extrusion printing methods with varying nozzle diameters using C2C12 cells. Following the results of this analysis, the viability data and printing parameters were used to compute shear stress for each print condition and develop a mathematical model to relate these variables to one another. Finally, prints with hMPCs – a more clinically relevant cell type in the context of TEMR constructs – were done to assess viability post-printing. This was done to begin to investigate potential discrepancies between the effects of printing on these different cell types.

Materials and Methods

Cell Culture

All C2C12 cells were cultured in 15cm petri dishes in DMEM changed every three days. These cells were cultured to 70% confluency before bioink preparation. All hMPCs were cultured in T75 flasks in human media changed every other day.

Bioink Preparation

2.5% HA in PBS was prepared by weighing out the HA powder and adding it into PBS in small increments while vortexing. The solution was mixed thoroughly with each increment before adding more HA. This solution was then refrigerated prior to use.

Prior to printing, cells were trypsinzed, centrifuged, counted, and then centrifuged again to be diluted in media at a seeding density of 4.9 million cells/mL. The desired volume of HA gel was then drawn up in a plunger syringe and the necessary volume of cell suspension to dilute the gel to 2% was drawn up into another syringe. The syringes were connected using the proper connector and the plungers were slowly pushed back and forth ten times to ensure even mixing. The plunger was then placed into a 50mL conical tube for sterile transport to the bioprinter. For pneumatic prints, the mixture was transferred to a pneumatic syringe using a connector.

Bioprinting

All prints were done on the CellInk BioX printer. Briefly, the printer and fan were turned on and then chamber cleaning was run. The proper printhead type and nozzle diameter options were selected based on the type of print. The infill density was set to 95% and the pattern was set to grid.

The print syringe was then loaded into the printhead and locked in. A manual calibration was run as well as an automatic homing cycle. The printhead was then manually adjusted to the desired start location and lowered until it is just above the print surface.

After printing was complete, the dishes or well plates were transported to an incubator and left for 90 minutes after which a few mL of cell culture media was added to each print. All prints were then incubated overnight prior to staining.

Fluorescent Staining & Cell Viability

One drop of DAPI stain per 1mL of media and one drop of Propidium Iodide stain per 1mL of media were mixed. 200uL of this mixture was then added to each print and the prints were incubated for 15-20 minutes prior to fluorescent imaging with a confocal microscope. DAPI stained all cell nuclei blue while Propidium Iodide stained dead cells red.

Cell viability was then quantified using ImageJ to count total cells and dead cells in each image and calculate the percentage of viable cells.

Rheometric Analysis

Rheometric analysis was performed on a sample of our specific HA formulation using a TA Instruments Hybrid Discovery HR-3 Rheometer. Briefly, the machine was calibrated prior to loading a 70uL sample of 2% HA solution in PBS. The resulting flow curve plotted viscosity (Pa·s) and strain (Pa) as a function of shear rate (1/s) and the raw data were exported to MATLAB R2018b for further modeling.

Mathematical Modeling

All mathematical modeling was performed on MATLAB R2018b and the built-in Curve Fitting Tool to perform regression analysis.

First, viscosity was plotted as a function of shear rate to closely assess the HA gel's non-Newtonian behavior. This would inform the rest of the modeling process including the maximum shear rate computation and, therefore the maximum shear stress computation.

Shear rate calculations were performed using principles derived from Newton's Law of Viscosity which is given as

$$\tau_{x,y} = \mu \frac{du}{dy} \quad [1]$$

where $\tau_{x,y}$ denotes the local shear stress, μ is the effective viscosity, and $\frac{du}{dy}$ describes the shear rate ($\dot{\gamma}$)and is the derivative of the fluid velocity.[15] Additionally, the bioink-syringe system was assumed to be a fully enclosed, cylindrical pipe with stationary boundaries, controlled flow rate, and a no-slip boundary condition. This also informed the computation of the maximum shear rate and, therefore the maximum shear stress.

Regression analysis was performed on shear stress as a function of shear rate, shear stress as a function of nozzle diameter, viability as a function of shear stress, and viability as a function of nozzle diameter. All regression models were then implemented in MATLAB functions to compute expected viability as well as expected maximum shear stress and strain for a given nozzle diameter and flow rate (Fig. S1).

Results

Initial printing with C2C12 cells was first performed using only the pneumatic printhead paired with either a 0.25mm-diameter nozzle or 0.41mm-diameter nozzle. These cells were printed onto dishes and slides in order to determine which surface would be optimal for staining and imaging going forward. The 0.41mm-diameter nozzle resulted in high average cell viability when printing on dishes (94.62%) and slides (95.84%). An unpaired T-test showed no significant difference between the average cell viability for both print surfaces (t(7)=1.1070, p=1.15). Additionally, the standard deviations for both print surface conditions were relatively small (0.92% and 0.94% for dish and slide prints respectively). In contrast, the 0.25mm-diameter nozzle prints were less consistent between print surface conditions with a dish viability average of 95.74% and a slide viability of only 76.75%. An unpaired T-test showed a significant difference between the average cell viability for both groups (t(9)=4.7493, p=0.0005). Higher standard deviations in cell viability were also observed with the 0.25mm-diameter nozzle (2.06% and 8.57% for dish and slide prints respectively). Ultimately, there were difficulties in staining and imaging the slides which led to our decision to proceed with dish printing for the rest of the project.

An initial print with the piston printhead paired with a 0.25mm-diameter nozzle and a 0.41mm-diameter nozzle yielded 98.28% and 98.19% cell viability for each nozzle respectively. An unpaired T-test showed no significant difference between the average cell viabilities for either nozzle size (t(18)=0.1310, p=0.449).

Quantitative Analysis with C2C12 cells

Next, we printed with pneumatic and piston printheads using both the 0.25mm- and 0.41mm-diameter nozzles for a total of four different print conditions each with four dishes. The 0.41mm-piston print had the highest average cell viability while the 0.41mm-pneumatic print had the lowest cell viability (Fig 2). An ANOVA test showed a significant difference between the averages of each print condition (F(3,12)=12.6173, p=0.0005). This was followed by Tukey's HSD test which indicated a significant

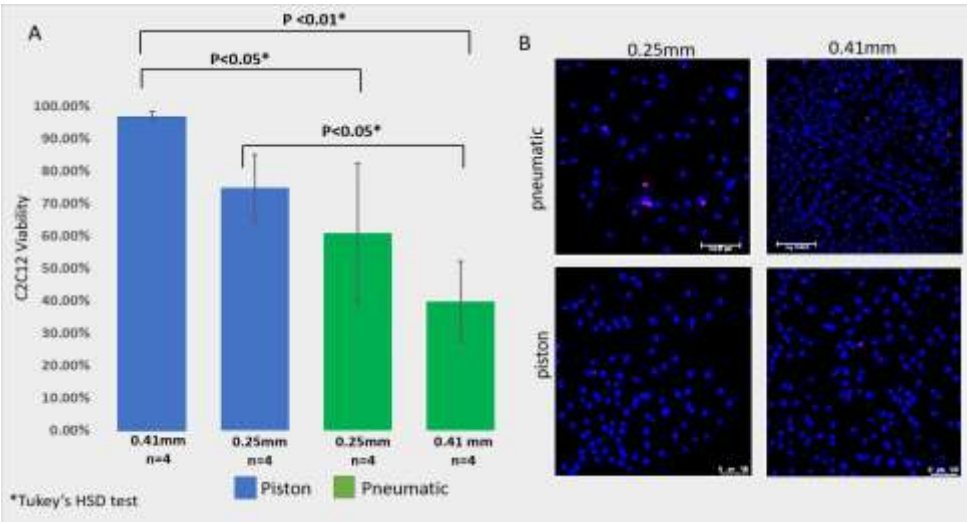

Fig. 2. C2C12 Viability with Different Printheads and Nozzle Sizes. (A) Average percent cell viability for each nozzle diameter and printhead type. P-values of significant post-hoc pair-wise comparisons are indicated. (B) Visual comparison of fluorescent cells printed with each nozzle diameter and printhead type. All cell nuclei are stained blue with DAPI while dead cells are stained red with propidium iodide. Higher incidence of cell death can be seen in both of the pneumatic prints as compared to the piston prints.

difference between the average cell viability for the 0.41mm-piston prints and the 0.25mm-pneumatic prints (Q=5.3147, p=0.013), the 0.41mm-piston prints and 0.41mm-pneumatic prints (Q=8.4473, p=0.001), as well the 0.25mm-piston prints and the 0.41mm-pneumatic prints (Q=5.2164, p=0.014).

Having observed a consistently high cell viability with the piston printhead, we decided to further investigate the differences in viability with more nozzle sizes using this printhead. This printing method was employed with four nozzle diameters (0.2mm, 0.25mm, 0.41mm, and 0.61mm). For each nozzle, a very high average cell viability (>99%) was achieved (Fig. 3). An ANOVA test showed no significant difference between the average cell viabilities for each nozzle size (F(3,31)=1.42488, p= 0.254)

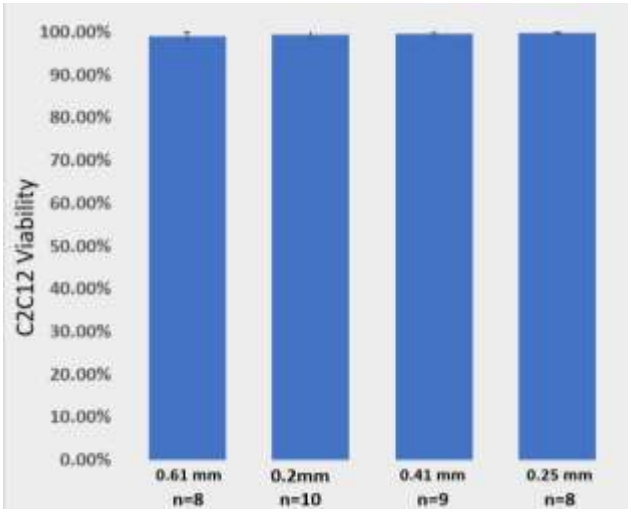

Fig. 3. C2C12 Viability with Varying Nozzle Sizes. Average percent cell viability for each nozzle diameter using the piston printhead. Very high cell viability was achieved for all nozzles. ANOVA test showed no significant difference between averages of each group (F(3,31)=1.42488, p= 0.254).

Mathematical Modeling

Having acquired data for multiple nozzle sizes paired with the piston printhead, we then moved on to our second specific aim of the project which was the mathematical modeling. Rheometric analysis of our 2% HA formulation provided stress and viscosity data as a function of shear rate which was then plotted to obtain a rheometric profile for the HA gel (Fig. 4A). The resulting curve indicated non-Newtonian behavior which is consistent with our expectations for HA.[16] Specifically, the viscosity decreased with increasing shear rate which indicated that our HA formulation was in fact a shear-thinning fluid (Fig. 4A). This was further confirmed by plotting viscosity as a function of shear rate using a logarithmic scale on both axes (Fig. S2). The resulting plot showed an approximately linear decrease in viscosity at higher shear rates – characteristic behavior of a shear-thinning fluid.[15,17]

Once the rheometric properties were characterized, regression analysis was performed on the stress data as a function of shear rate (Fig. 4B). The power-law model was used as this is the simplest fit for shear-thinning fluids.[15,17] The general regression model can be seen in Equation 2

$$f(x) = ax^b \qquad [2]$$

where *f(x)* is stress as a function of shear rate ($\tau(\dot{\gamma})$), *a* corresponds to the flow consistency index (*K*), and *b* corresponds to the flow behavior index (*n*). The regression analysis yielded values of 24.29 and 0.2738 for *K* and *n* respectively ($R^2 = 0.9801$). Therefore, the following equation was then implemented in a MATLAB function to compute stress given shear rate (Fig. S1).

$$\tau(\dot{\gamma}) = 24.29\dot{\gamma}^{0.2738} \qquad [3]$$

Similarly, a power regression was applied to the viscosity data as a function of shear rate (Fig. S2) (R^2 =

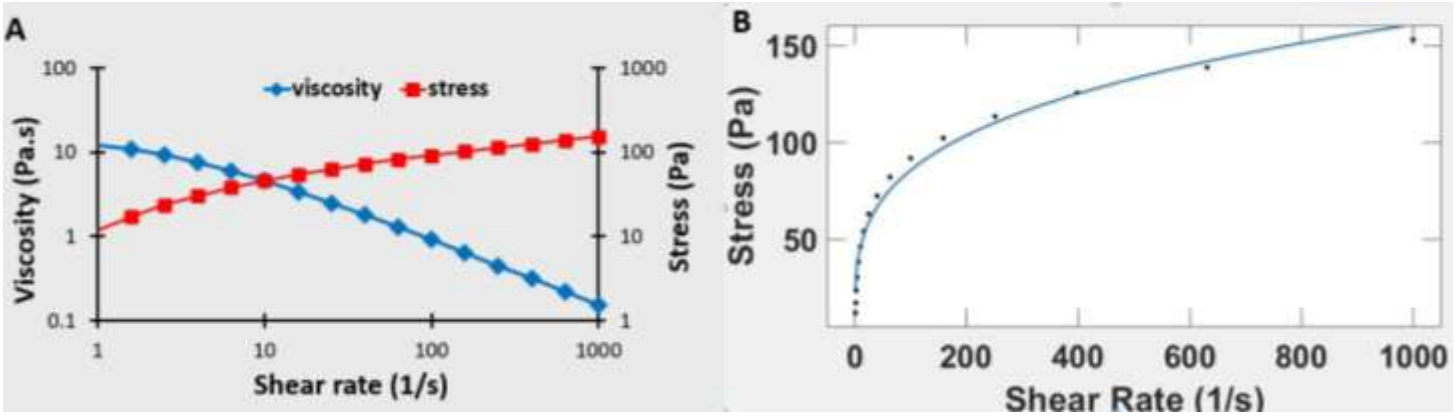

Fig. 4. Rheometric Analysis and Regression Analysis of Stress. (A) Log-log plot of viscosity and stress as a function of shear rate. (B) Plot of stress as a function of shear rate with a power law regression imposed (R^2 = 0.9801).

0.9785). This regression model was then implemented in a MATLAB function which takes shear rate as an input and computes the corresponding viscosity.

Next, the maximum shear rate was computed for each of the four nozzle diameters with which C2C12 cells were printed. As previously mentioned, for unidirectional fluid flow in a pipe, shear rate is the derivative of the velocity profile. For a Newtonian fluid with n = 1, this velocity profile is quadratic. In comparison, the flow of a shear-thinning fluid (n < 1) is flatter in the middle and quickly decreases towards the boundary where viscosity is low and stress is high. This can be seen in Figure S3 which depicts velocity profiles and the shear rate profile for fluid flow in a pipe. Since we are interested in the maximum stress upon the cells during the printing process, we consider the shear rate at the boundary, where shear rate is highest, in order to compute stress. We used the following formula for shear rate at the wall of fluid flowing through a pipe which is derived from the parabolic velocity profile and the relationship between linear velocity and volumetric flow rate

$$\dot{\gamma}_{max} = \frac{4Q}{\pi r^3} \qquad [4]$$

where Q is the volumetric flow rate and r is the inner radius of the pipe. The flow rate for all prints was set to 08. uL/s because this rate was found to consistently push out ink for all nozzle sizes. A MATLAB function implemented Equation 4 along with the constant flow rate and varying nozzle diameters to compute the theoretical maximum wall shear rate for each nozzle size. Then, the MATLAB function implementing Equation 3 was used to calculate the theoretical maximum stress for each nozzle size.

Additionally, from Equation 1 and Equation 4, it was expected that a rational regression model would be a good fit for stress as a function of nozzle diameter. As such, regression analysis was done on the data in order to have a visual representation of the relationship between decreasing nozzle diameters and increasing stress using the following equation

$$f(x) = \frac{p_1}{x^3 + q_1 x^2 + q_2 x + q_3} \qquad [5]$$

where $f(x)$ is stress, x is nozzle diameter, and p_1 & q_{1-3} are constants. As expected, shear stress decreased with increasing nozzle diameter (Fig. 5A). The regression yielded values of 78.89, -1.993, 4.429, and 0.1018 for constants p_1, q_1, q_2, and q_3 respectively (R^2 = 1).

The next step in the modeling process was to perform regression analyses on C2C12 average cell viability data as a function of stress and nozzle size. The data were fitted by imposing a linear regression model

$$f(x) = ax + b \qquad [6]$$

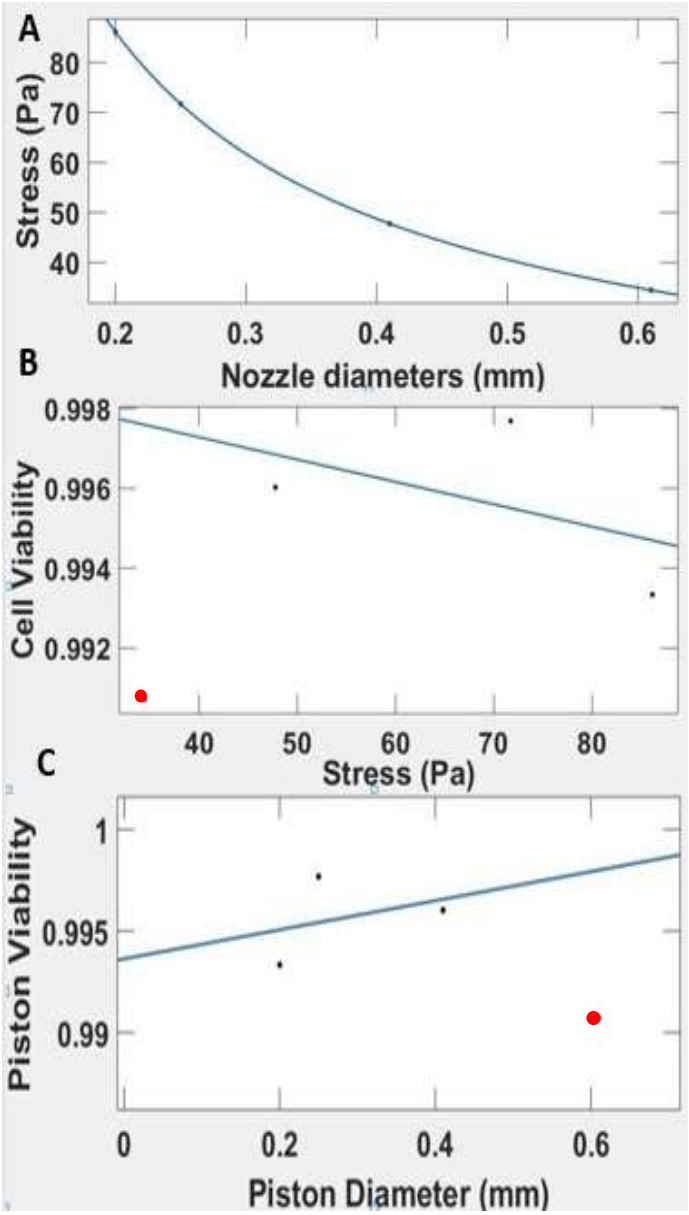

Fig. 5. Regression Analyses. (A) Plot of stress as a function of nozzle diameter with rational regression imposed (R^2 = 1). (B) Plot of cell viability as a function of stress with linear regression imposed (R^2 = 0.128). The red dot indicates the data point which was excluded. (C) Plot of cell viability as a function of snozzle diameter with linear regression imposed (R^2 = 0.244). The red dot indicates the data point which was excluded (F(2,19)=0.31867l, p=0.731).

where *f(x)* is the cell viability fraction, *x* is nozzle diameter (mm), and *a* and *b* are constants. For viability as a function of stress, the regression yielded values of -5.598×10^{-5} and 0.9995 for constants *a* and *b* respectively ($R^2 = 0.128$). For viability as a function of nozzle diameter, the regression yielded values of 0.007156 and 0.9936 for constants *a* and *b* respectively ($R^2 = 0.244$). Both resulting regression equations were implemented in MATLAB functions which compute cell viabilities given a nozzle diameter or shear stress (Fig. S1). Based on the current understanding of the effects of shear stress on cell integrity as well as the previously observed relationship between nozzle size and stress, we expected to see a positive correlation between cell viability and nozzle diameter and a negative correlation between cell viability and stress. Thus, when imposing the linear regression described by Equation 6, we excluded one data point in each plot which skewed the line of best fit away from the expected trend (Fig. 5).

hMPCs Printing

Having observed high C2C12 cell viability with the piston printhead paired with a 0.41mm-diameter nozzle, hMPCs were printed on three plates using this same combination. Very high cell viability (>98%) was achieved for all replicates (Fig. 6). An ANOVA test showed no significant difference between the averages for each plate ($F(2,19)=0.31867$l, $p=0.731$).

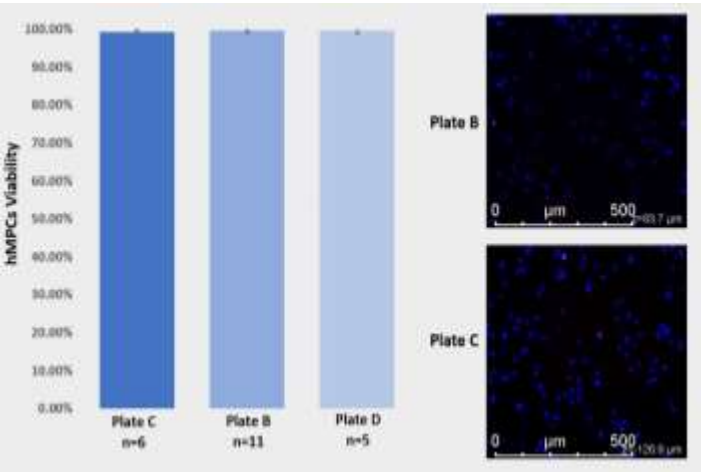

Fig. 6. hMPCs Viability. (A) Average cell viability of hMPCs printed on three plates. ANOVA showed no significant difference between groups ($F(2,19)=0.31867$l, $p=0.731$). (B) Visual comparison of fluorescent cells from two dishes. All cell nuclei are stained blue with DAPI while dead cells are stained red with propidium iodide. Very low incidence of cell death is observed.

Discussion

Printing C2C12 cells using either pneumatic or piston printheads suggested that piston-driven extrusion more consistently yielded high cell viability. First, the initial prints with the piston printhead using two nozzle sizes yielded higher average cell viability than the previous prints using pneumatic printheads. This observation was further supported by the results seen in Figure 2 where the 0.41mm-piston print had a much higher viability than the 0.41mm-penumatic print ($P<0.01$) and the 0.25mm-pneumatic print ($P<0.05$). Additionally, the 0.25mm-piston print had a higher average viability than the 0.41mm-pneumatic print ($P<0.05$). These results support the idea that the steady extrusion and consistent deposition of bioink from a mechanically driven printhead may provide benefits over the pneumatic printhead in terms of cell viability. The results from the BioX printer also provide some evidence to explain how the Organovo NovoGen printer – a piston-driven extrusion system – is able to achieve viability as high as ~98% with muscle progenitor cells.[2] Additionally, achieving consistently high cell viability with four different nozzle diameters ranging from 0.2mm to 0.61mm further supports the use of a piston-printhead when seeking the highest possible cell viability. However, it is important to note that high cell viabilities were achieved with the pneumatic printhead as well which are more commercially available and user-friendly.

The absence of a significant difference between piston-driven prints with four different nozzle diameters could indicate that the ranges of nozzles was not broad enough to observe the expected effect of nozzle diameter (and consequently shear stress) on cell viability. The limited availability of nozzle diameters for testing restricted the amount of data points that could be fitted using a linear regression. Therefore, the models derived from the data need to be confirmed with more prints and improved by using more nozzle sizes. This limitation was also made apparent by the need to exclude a data point in the regression analyses. This was done in order to achieve a trend line that matched the expected relationship between shear stress and cell viability. Therefore, the goodness of fit of the reported models was low. Furthermore, since the extrusion rate was kept constant at 0.8uL/s for all nozzle diameters, the bioink deposition was inconsistent across prints. This resulted in different volumes of bioink between groups which may have had a significant impact on differences in cell counts and therefore cell viability.

The reason for using C2C12 cells was their clinical relevance in the context of TEMR for treating VML. Unfortunately, lot-to-lot variability in growth kinetics as

well as other technical difficulties in optimizing the printing procedure limited our work with hMPCs. However, the very high cell viability achieved using this cell type highlights the potential of bioprinting as a tool in TEMR fabrication. As an immortalized lab cell line, C2C12 cells are a more a more robust cells and therefore likelier to withstand the stresses involved in the bioprinting process. As such, the effects of this process on cell viability are likely exacerbated when using hMPCs. More work using hMPCs with different nozzle diameters is needed to derive mathematical models relevant to these cell types. Comparing the effects of different nozzle diameters and print methods across both cell types could provide insights into how the printing process effects these cells differently. Additionally, the mathematical modeling process outlined above demonstrates that the stresses to which cells are subjected during printing are largely dependent on the hydrogel being used. The use of a 2% HA formulation with muscle progenitor cells gives this project relevance in the context of TEMR for VML treatment. However, future work could include the use of other hydrogels to investigate how rheometric characteristics factor into biocompatibility.

Our quantitative analysis did provide evidence of the variability in cell viability outcomes between printing methods. This corroborates the discrepancies apparent across other relevant studies using bioprinting with different cell types (Table 1). This variability has important implications in the application of bioprinting for biofabrication of tissue engineering medical products (TEMPs) of which TEMR constructs are an example. Full understanding and control over the manufacturing process are crucial considerations towards ensuring reproducibility, functionality, and safety. To this end, it is necessary to determine a benchmark cell viability that serves as a critical quality attribute needed for TEMR functionality. This extends to other TEMPs as well which is why other non-muscle human cell types are included in Table 1 such as endothelial cells and fibroblasts. While it is clear that high cell viability can be achieved with the right combination of print parameters, using bioprinting as a TEMR biomanufacturing tool will require rigorous standards and constraints. Differences as large as >30% cell viability, as seen in this project as well as in Table 1, need to be accounted for and understood. For example, achieving 85% cell viability for a particular print surpasses the ISO standard for implanted medical devices but there should be strong rationale for the implantation of the remaining 15% which are dead. Therefore, this project serves as an initial quantitative analysis of the differences in cell viability observed between print methods and nozzle size as it relates to shear stress with mathematical models to represent these relationships.

Cell Types	Post-Print Viability (Time delay)	Printing System
Human mesenchymal progenitor cells[18]	86.4±3.5% (24hr)	Pneumatic
Mesenchymal stem cells[19]	89±2% (5hr)	Pneumatic
Human aortic valve interstitial cells [20]	>90% (3 days)	Piston
Human aortic root smooth muscle cells[21]	81.4±3.4% (7 days)	Piston
Human fetal cardiomyocyte progenitor cells[22]	92% and 88% (24hr)	Pneumatic
Human neonatal derma fibroblast cells[23]	70% and 61% (0 days)	Pneumatic
Human urothelial cells[24]	85±2% (1 day)	Pneumatic
Human umbilical vein endothelial cells[24]	93±2% (0 days)	Pneumatic
Human adipose derived stem cells[25]	92.6±5.18% and 83.62±2.78%	Piston
Human corneal epithelial cells[26]	94.6 +/- 2.5%	Pneumatic
C2C12 myoblasts[27]	94.0±1.0% (24hr)	Pneumatic
C2C12[28]	>85%	Pneumatic

Table. 1. Variations in Reported Cell Viability. Cell viability values from different studies using extrusion-based bioprinting to print human cells. The cell type and printhead type are also included and the time delay between printing and cell viability assessment is indicated in parentheses. Two studies which used C2C12 cells are also included. This small sample highlights the range and deviation in reported viability.

End Matter

Acknowledgements
Dr. George Christ, Ph.D. and Dr. Chris Highley, Ph.D. for guidance and advising throughout the project.

Sydney Shriver for guidance and performing all laboratory work throughout the project.

References

1. Derakhshanfar, S. *et al.* 3D bioprinting for biomedical devices and tissue engineering: A review of recent trends and advances. *Bioact. Mater.* **3**, 144–156 (2018).
2. Bour, R. K. *et al.* Bioprinting on sheet-based scaffolds applied to the creation of implantable tissue-engineered constructs with potentially diverse clinical applications: Tissue-Engineered Muscle Repair (TEMR) as a representative testbed. *Connect. Tissue Res.* **61**, 216–228 (2020).
3. An overview of extrusion-based bioprinting with a focus on induced shear stress and its effect on cell viability. *Bioprinting* **20**, e00093 (2020).
4. Murphy, S. V. & Atala, A. 3D bioprinting of tissues and organs. *Nat. Biotechnol.* **32**, 773–785 (2014).
5. Cidonio, G., Glinka, M., Dawson, J. I. & Oreffo, R. O. C. The cell in the ink: Improving biofabrication by printing stem cells for skeletal regenerative medicine. *Biomaterials* **209**, 10–24 (2019).
6. Fisch, P., Holub, M. & Zenobi-Wong, M. Improved accuracy and precision of bioprinting through progressive cavity pump-controlled extrusion. *bioRxiv* 2020.01.23.915868 (2020) doi:10.1101/2020.01.23.915868.
7. Gungor-Ozkerim, P. S., Inci, I., Zhang, Y. S., Khademhosseini, A. & Dokmeci, M. R. Bioinks for 3D bioprinting: an overview. *Biomater. Sci.* **6**, 915–946 (2018).
8. Grogan, B. F., Hsu, J. R. & Consortium, S. T. R. Volumetric Muscle Loss. *JAAOS - J. Am. Acad. Orthop. Surg.* **19**, S35 (2011).
9. Ning, L., Betancourt, N., Schreyer, D. J. & Chen, X. Characterization of Cell Damage and Proliferative Ability during and after Bioprinting. *ACS Biomater. Sci. Eng.* **4**, 3906–3918 (2018).
10. Zhao, Y., Li, Y., Mao, S., Sun, W. & Yao, R. The influence of printing parameters on cell survival rate and printability in microextrusion-based 3D cell printing technology. *Biofabrication* **7**, 045002 (2015).
11. Lepowsky, E., Muradoglu, M. & Tasoglu, S. Towards preserving post-printing cell viability and improving the resolution: Past, present, and future of 3D bioprinting theory. *Bioprinting* **11**, e00034 (2018).
12. Nair, K. *et al.* Characterization of cell viability during bioprinting processes. *Biotechnol. J.* **4**, 1168–1177 (2009).
13. ISO 10993-5:2009(en), Biological evaluation of medical devices — Part 5: Tests for in vitro cytotoxicity. https://www.iso.org/obp/ui/#iso:std:iso:10993:-5:ed-3:v1:en.
14. Pedde, R. D. *et al.* Emerging Biofabrication Strategies for Engineering Complex Tissue Constructs. *Adv. Mater.* **29**, (2017).
15. Yao, L.-S., Mamun Molla, Md. & Ghosh Moulic, S. Fully-Developed Circular-Pipe Flow of a Non-Newtonian Pseudoplastic Fluid. *Univers. J. Mech. Eng.* **1**, 23–31 (2013).
16. Pisárčik, M., Bakoš, D. & Čeppan, M. Non-Newtonian properties of hyaluronic acid aqueous solution. *Colloids Surf. Physicochem. Eng. Asp.* **97**, 197–202 (1995).
17. Boger, D. V. Demonstration of upper and lower Newtonian fluid behaviour in a pseudoplastic fluid. *Nature* **265**, 126–128 (1977).
18. Modeling of the Flow Rate in the Dispensing-Based Process for Fabricating Tissue Scaffolds | Journal of Manufacturing Science and Engineering | ASME Digital Collection. https://asmedigitalcollection.asme.org/manufacturingscience/article/130/2/021003/462176/Modeling-of-the-Flow-Rate-in-the-Dispensing-Based.
19. Blaeser, A. *et al.* Controlling Shear Stress in 3D Bioprinting is a Key Factor to Balance Printing Resolution and Stem Cell Integrity. *Adv. Healthc. Mater.* **5**, 326–333 (2016).
20. Kim, J. H. *et al.* 3D Bioprinted Human Skeletal Muscle Constructs for Muscle Function Restoration. *Sci. Rep.* **8**, 12307 (2018).
21. 3D Bioprinting of Heterogeneous Aortic Valve Conduits with Alginate/Gelatin Hydrogels. https://www-ncbi-nlm-nih-gov.proxy01.its.virginia.edu/pmc/articles/PMC3694360/.
22. 3D Bioprinting of Vascularized, Heterogeneous Cell-Laden Tissue Constructs - Kolesky - 2014 - Advanced Materials - Wiley Online Library. https://onlinelibrary.wiley.com/doi/full/10.1002/adma.201305506?casa_token=3nivq5aTD0EAAAAA%3AydcFb24Kunfo5ztAH6SaBk7TjOcuw_8zI2f3tAyXPJI29J-5TI4Mby-MyV0rM0mTx5URrk0ul9VVd7-j.
23. Fedorovich, N. E. *et al.* Biofabrication of Osteochondral Tissue Equivalents by Printing Topologically Defined,

Cell-Laden Hydrogel Scaffolds. *Tissue Eng. Part C Methods* **18**, 33–44 (2012).
24. Bioprinting three-dimensional cell-laden tissue constructs with controllable degradation | Scientific Reports. https://www-nature-com.proxy01.its.virginia.edu/articles/srep24474?report=reader.
25. Gaetani, R. *et al.* Cardiac tissue engineering using tissue printing technology and human cardiac progenitor cells. *Biomaterials* **33**, 1782–1790 (2012).
26. Mozetic, P., Giannitelli, S. M., Gori, M., Trombetta, M. & Rainer, A. Engineering muscle cell alignment through 3D bioprinting. *J. Biomed. Mater. Res. A* **105**, 2582–2588 (2017).
27. Frontiers | Microtissues Enhance Smooth Muscle Differentiation and Cell Viability of hADSCs for Three Dimensional Bioprinting | Physiology. https://www.frontiersin.org/articles/10.3389/fphys.2017.00534/full.
28. Duan, B., Kapetanovic, E., Hockaday, L. A. & Butcher, J. T. Three-dimensional printed trileaflet valve conduits using biological hydrogels and human valve interstitial cells. *Acta Biomater.* **10**, 1836–1846 (2014).

Supplemental Figures

```
function [viscosity] = calc_viscosity(shear_rate)
% This function takes shear rate as an input and computes the correspondin
% viscosity as determined by a power law regression model unique to our
% HA formulation
viscosity = 13.13*(shear_rate^-0.4769);
end
function [shear_rate] = calc_shear_rate(nozzle_diameter, flow_rate)
% This function takes nozzle diameter and flow rate as inputs and computes
% the corresponding maximum shear rate as determined by derivtaive of the
% velocity profile of a fluid moving through a fully enclosed,
% cylindrical pipe with stationary boundaries, controlled flow rate, and a
% no-slip boundary condition at the wall
radius = (nozzle_diameter/2)/1000; % convert diamet er(mm) to radius(m)
flow_rate = flow_rate*(10^-10); % convert flow rate from uL/s to m^3/s
shear_rate = 4*(flow_rate)./(pi*(radius.^3));
end
function [max_shear_stress] = calc_stress(shear_rate)
% This function takes shear rate as an input and computes the correspondin
% shear stress as determined by a power law regression model unique to our
% HA formulation
max_shear_stress =24.29.*(shear_rate.^0.2738);
end
function [viability] = stress_to_viability(shear_stress)
% This function takes nozzle diameter as an input and computes the
% expected cell viability as determined by a regression regression model
viability = -0.002412.*(shear_stress.^2) + 0.02668.*shear_rate + 0.9244;
end
function [viability] = nozzle_to_viability(nozzle_diameter)
% This function takes nozzle diameter as an input and computes the
% expected cell viability as determined by a regression regression model
viability = -0.1025.*(nozzle_diameter.^2) + 0.07331.*shear_rate + 0.964;
end
function [shear_stress] = nozzle_to_stress(nozzle_diameter, flow_rate)
% This function takes nozzle diameter as an input and computes the
% expected shear stress as determined by other functions
shear_stress = calc_stress(calc_shear_rate(nozzle_diameter, flow_rate));
end
```

Fig. S1. MATLAB Functions. All MATLAB functions referenced in the text are included here along with documentation describing the inputs, outputs, and computations. From top to bottom they perform the following computations: calculating viscosity given shear rate, calculating shear rate given nozzle diameter and flow rate, calculating stress given shear rate, calculating viability given stress, calculating viability given nozzle diameter, and calculating stress given nozzle diameter.

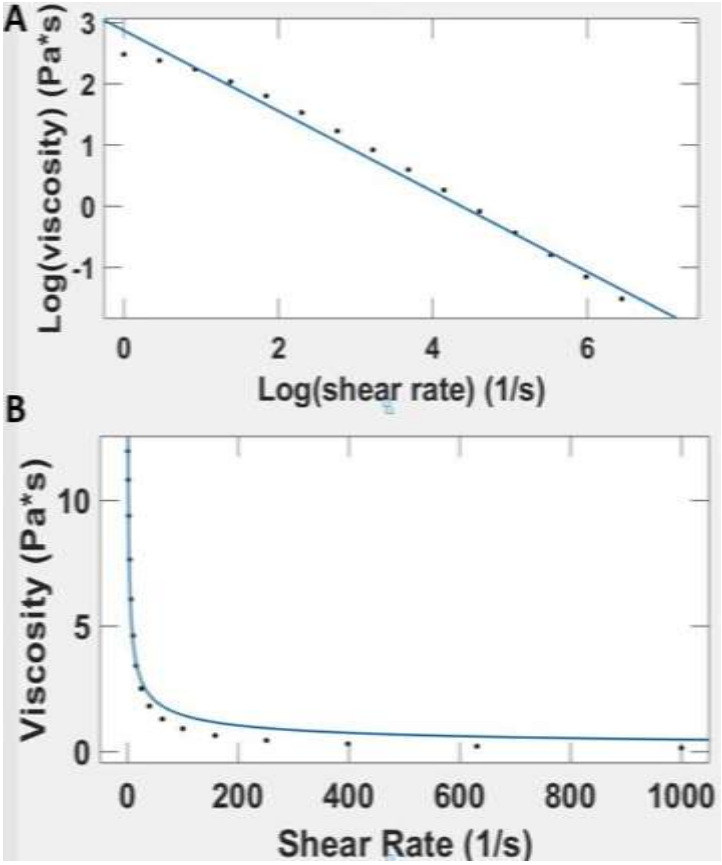

Fig. S2. Viscosity vs Shear Rate with Regression. (A) Log-log plot of viscosity as a function of shear rate with a linear regression imposed. This plot depicts the shear-thinning behavior of 2% HA ($R^2 = 0.9868$). (B) Plot of viscosity as a function of shear rate with a power law regression model imposed ($R^2 = 0.9785$).

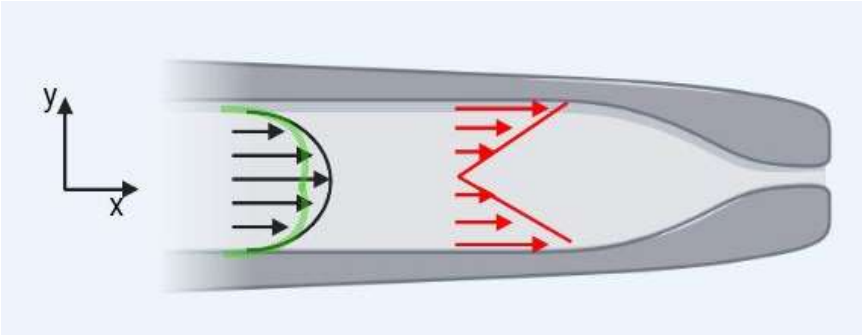

Fig. S3. Fluid Flow Profiles in a Cylindrical Pipe. The black arrows represent a Newtonian fluid's velocity profile while the green arc represents a possible power law fluid velocity profile. The red arrows represent the shear rate – the derivative of the velocity profile – for the Newtonian fluid. (Created with BioRender.com)